JNS

CLINICAL ARTICLE

Intraoperative application and early experience with novel high-resolution, high-channel-count thin-film electrodes for human microelectrocorticography

Hao Tan, BS,[1] Angelique C. Paulk, PhD,[2,3] Brittany Stedelin, BS,[1] Daniel R. Cleary, MD, PhD,[1,4] Caleb Nerison, BS,[1] Youngbin Tchoe, PhD,[5,6,10] Erik C. Brown, MD, PhD,[1,7] Andrew Bourhis, MS,[5] Samantha Russman, MS,[5] Jihwan Lee, MS,[5] Karen J. Tonsfeldt, PhD,[5,8] Jimmy C. Yang, MD,[2,3] Hongseok Oh, PhD,[5,9] Yun Goo Ro, PhD,[5,9] Keundong Lee, PhD,[5] Mehran Ganji, PhD,[5] Ian Galton, PhD,[5] Dominic Siler, MD, PhD,[1] Seunggu Jude Han, MD,[12] Kelly L. Collins, MD,[1,11] Sharona Ben-Haim, MD,[4] Eric Halgren, PhD,[13] Sydney S. Cash, MD, PhD,[2,3] Shadi Dayeh, PhD,[5] and Ahmed M. Raslan, MD[1]

[1]Department of Neurological Surgery, Oregon Health & Science University, Portland, Oregon; [2]Department of Neurology, Massachusetts General Hospital, Boston, Massachusetts; [3]Harvard Medical School, Boston, Massachusetts; Departments of [4]Neurological Surgery, [5]Electrical and Computer Engineering, and [13]Neurology, University of California, San Diego, California; [6]Department of Biomedical Engineering, Ulsan National Institute of Science and Technology, Ulsan, Korea; [7]Department of Neurological Surgery, Nicklaus Children's Hospital, Miami, Florida; [8]Department of Obstetrics, Gynecology, and Reproductive Sciences, Center for Reproductive Science and Medicine, University of California, San Diego, La Jolla, California; [9]Soongsil University, Seoul, Korea; [10]Ulsan National Institute of Science and Technology, Ulsan, Korea; [11]Papé Family Pediatric Research Institute, Oregon Health & Science University, Portland, Oregon; and [12]Department of Neurological Surgery, Stanford University, Palo Alto, California

OBJECTIVE The study objective was to evaluate intraoperative experience with newly developed high-spatial-resolution microelectrode grids composed of poly(3,4-ethylenedioxythiophene) with polystyrene sulfonate (PEDOT:PSS), and those composed of platinum nanorods (PtNRs).

METHODS A cohort of patients who underwent craniotomy for pathological tissue resection and who had high-spatial-resolution microelectrode grids placed intraoperatively were evaluated. Patient demographic and baseline clinical variables as well as relevant microelectrode grid characteristic data were collected. The primary and secondary outcome measures of interest were successful microelectrode grid utilization with usable resting-state or task-related data, and grid-related adverse intraoperative events and/or grid dysfunction.

RESULTS Included in the analysis were 89 cases of patients who underwent a craniotomy for resection of neoplasms (n = 58) or epileptogenic tissue (n = 31). These cases accounted for 94 grids: 58 PEDOT:PSS and 36 PtNR grids. Of these 94 grids, 86 were functional and used successfully to obtain cortical recordings from 82 patients. The mean cortical grid recording duration was 15.3 ± 1.15 minutes. Most recordings in patients were obtained during experimental tasks (n = 52, 58.4%), involving language and sensorimotor testing paradigms, or were obtained passively during resting state (n = 32, 36.0%). There were no intraoperative adverse events related to grid placement. However, there were instances of PtNR grid dysfunction (n = 8) related to damage incurred by suboptimal preoperative sterilization (n = 7) and improper handling (n = 1); intraoperative recordings were not performed. Vaporized peroxide sterilization was the most optimal sterilization method for PtNR grids, providing a significantly greater number of usable channels poststerilization than did steam-based sterilization techniques (median 905.0 [IQR 650.8–935.5] vs 356.0 [IQR 18.0–597.8], p = 0.0031).

CONCLUSIONS High-spatial-resolution microelectrode grids can be readily incorporated into appropriately selected craniotomy cases for clinical and research purposes. Grids are reliable when preoperative handling and sterilization con-

ABBREVIATIONS BCI = brain–computer interface; BWH = Brigham and Women's Hospital; ECoG = electrocorticography; HGA = high gamma activity; HGM = high gamma mapping; MGH = Massachusetts General Hospital; M1-S1 = primary motor cortex–primary sensory cortex; OHSU = Oregon Health & Science University; OR = operating room; PEDOT:PSS = poly(3,4-ethylenedioxythiophene) with polystyrene sulfonate; PtNR = platinum nanorod; SSEP = somatosensory evoked potential; STG = superior temporal gyrus; UCSD = University of California, San Diego; V-PRO = vaporized peroxide.

SUBMITTED April 28, 2023. **ACCEPTED** July 18, 2023.
INCLUDE WHEN CITING Published online September 29, 2023; DOI: 10.3171/2023.7.JNS23885.

siderations are accounted for. Future investigations should compare the diagnostic utility of these high-resolution grids to commercially available counterparts and assess whether diagnostic discrepancies relate to clinical outcomes.

https://thejns.org/doi/abs/10.3171/2023.7.JNS23885

KEYWORDS mapping; intraoperative; electrocorticography; gamma band; passive; high resolution; cortical; functional neurosurgery

Intraoperative functional cortical localization is critical for achieving successful outcomes after brain surgery. Several methods are used to achieve such outcomes—including preoperative functional imaging studies and intraoperative neurophysiological testing through techniques such as somatosensory evoked potential (SSEP) phase reversal for central sulcus localization, direct electrical cortical stimulation mapping, and subcortical stimulation.[1,2] More recently, intraoperative passive high gamma mapping (HGM; 70–170 Hz) has emerged as a viable method for localizing functional cortical regions without electrical stimulation.[3,4] This has been shown potentially to help better inform intraoperative surgical decision-making.[5,6]

Passive HGM relies on electrocorticography (ECoG) performed using subdural strips or grids. Current commercially available US FDA–approved clinical ECoG grids have spatial resolution constraints in the form of 10-mm pitch on average with an electrode density of 1 electrode/cm^2, although higher-density clinical grids can be condensed below an interelectrode distance (pitch) of 4 mm to improve resolution.[7] Furthermore, these grids are situated on a plastic mold that has difficulty conforming to the cortical surface without manual placement, which in our experience can cause discomfort to patients during awake procedures (our personal observations, 2020).

In light of these limitations, a 4-institution research collaboration between Oregon Health & Science University (OHSU); University of California, San Diego (UCSD); Massachusetts General Hospital (MGH); and Brigham and Women's Hospital (BWH) has developed ECoG grids composed of thin-film poly(3,4-ethylenedioxythiophene) with polystyrene sulfonate (PEDOT:PSS) and platinum nanorods (PtNRs).[8,9] These material compositions circumvent the limitations of existing clinical ECoG designs, and allow for higher spatial resolution (44–100/cm^2) and improved delineation of cortical regions of functional importance.[10–12]

Here we describe our collected experience with using high-spatial-resolution PEDOT:PSS and PtNR grids for cortical surface recording. The primary and secondary outcome measures in patients who underwent a craniotomy procedure were successful microelectrode grid utilization with usable resting-state or task-related data, and grid-related adverse intraoperative events and/or grid dysfunction. An overview of procedural considerations related to grid use for neurosurgeons is also provided.

Methods

Study Design and Patient Selection

Data were obtained in all adult patients who consented to the placement of high-resolution microelectrode grids during a craniotomy for resection of pathological tissue. Data were collected between January 1, 2019, and September 10, 2021, for both PEDOT:PSS grids and PtNR grids, and through April 1, 2022, for PEDOT:PSS grids at OHSU, UCSD, BWH, and MGH. This study was approved by the institutional review boards at all participating institutions (SMART IRB); subject consent was obtained. Strengthening the Reporting of Observational Studies in Epidemiology (STROBE) reporting guidelines were followed.[13]

Demographic, Clinical, and Intraoperative Variables

Demographic variables of interest included age and sex. Clinical variables of interest included indication for surgery, institution where surgery and grid placement were performed, and preoperative functional deficits. Intraoperative variables of interest included type of anesthesia and clinical mapping modalities used.

Microelectrode Grid Characteristics of Interest and Outcome Measures

Microelectrode grid data included chemical composition, number of channels, microelectrode placement strategy, and intracranial location of microelectrode placement. Electrophysiology data collected during recordings were as previously reported.[10–12,14] Successful use of grids for cortical recording, presence of intraoperative complications and adverse events related to grid use, and instances of microelectrode dysfunction and failure served as primary and secondary outcomes of interest. Additionally, adverse event data included instances of intraoperative cortical tissue damage following grid use, evidence of tissue damage on immediate postoperative imaging studies, and infection within 90 days after surgery.

PEDOT:PSS and PtNR Grid Chemical Composition and Configuration

Electrode grids were PEDOT:PSS and PtNR grids (Fig. 1). Specifications and nuanced differences between grids' specific material compositions are as previously published.[10] In summary, PEDOT:PSS grids are composed of thin-film poly(3,4-ethylenedioxythiophene) with polystyrene sulfonate. PtNR grids are composed of elemental platinum, the most widely used biocompatible electrode material, and offer greater stability in vivo.[9,15] Grids measuring 32 × 32 mm were composed of 1024 channels. Grids measuring 48 × 48 mm with 2048 channels were used in 2 cases. Grids with 128 channels had 3 conformations: 1) two 64-channel columns with 50-μm pitch; 2) two 64-channel columns with 800-μm pitch; and 3) a 4-mm-diameter circular grid.[12]

Microelectrode Grid Handling

All microelectrode grids were custom-manufactured at the UCSD Integrated Electronics and Biointerfaces

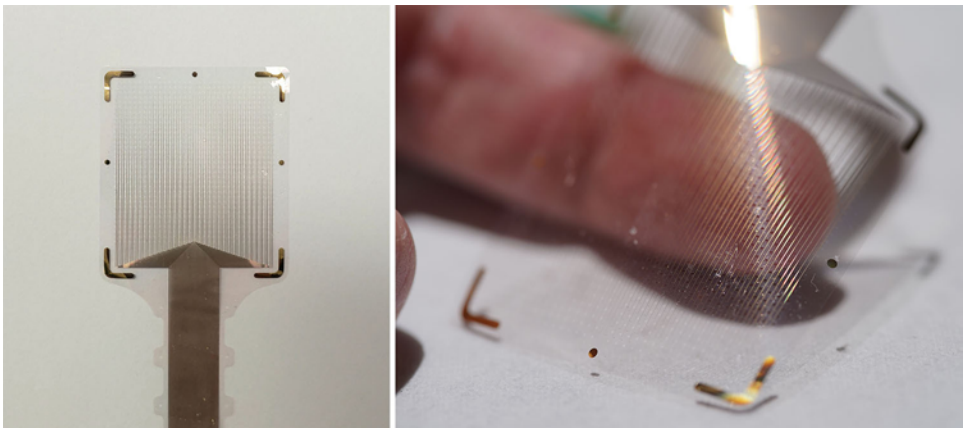

FIG. 1. Photographs of exemplar microelectrode grids (specifically PtNR grids) used. **Left:** Note how the electrode contacts are invisible to the naked eye. **Right:** Photograph of the grid relative to a finger to provide a sense of how compact the microelectrode contacts are. Figure is available in color online only.

Laboratory (IEBL) and received within 2 weeks of an order request. Given microelectrode grid malleability and its delicate nature, electrodes were packaged securely in DuraHolder Instrument Protection System (Key Surgical) pouches to minimize mechanical damage during the shipping process (Fig. 2A). Once received, grids were typically stored within the packaging material, in a temperate environment with low to moderate humidity (between 50°F and 75°F), until use.

Microelectrode grids were maintained on a flat surface to prevent damage before and during transportation for sterilization or to the operating room (OR). If a microelectrode grid was handled, staff were advised and trained to hold it vertically by the bonded extension board so that the microelectrode grid was suspended downward. In this way, unwanted contact between any given electrode and the immediate surroundings was minimized (Fig. 2B).

Microelectrode Grid Sterilization

Microelectrode grid sterilization techniques have been described previously.[10,16] Following the method of Uguz et al. published in 2016,[16] PEDOT:PSS grids were steam sterilized with a steam-based gravity cycle in the autoclave at 250°F/121°C for 30 minutes followed by at least 20 minutes of dry time. For PtNR grids, a 28-minute nonlumen vaporized peroxide (V-PRO) cycle, which involves aerosolization of hydrogen peroxide, was used. PtNR grids in their DuraHolder pouches were placed on a 470 × 274 × 90–mm anodized tray with perforated bottoms enclosed within a SterilContainer system (Aesculap Surgical Technologies), allowing 2 grids to be sterilized simultaneously per cycle (Fig. 2A). Electrode grids were typically used within 6 days of sterilization.

OR Preparation

Sterilized grids were transferred to a Mayo Stand and the extension board was inserted through an approximately 10-cm opening within the Situate Sterile Drape (Fig. 2B). Another smaller opening was created to pass touchproof connectors for a pair of sterile subdermal needle electrodes, which serve as separate reference and ground electrodes placed in the temporalis muscle or scalp. Then, Tegaderm was used to securely seal the drape openings (Fig. 2B). While sterile staff engaged in sterile technique to secure the sterile component of the extension board in place, another nonsterile member of the team on the other side of the drape connected the extension board to an amplifier board (Fig. 2C). The drape was then pulled by a nonsterile member of the team over the amplifier board and its outgoing serial peripheral interface cables (Fig. 2D). Channel yield and impedance testing was then performed prior to placement (Fig. 2E). Once the electrode was satisfactorily positioned over cortical regions of interest, Greenberg or C clamps were fastened to the acquisition board to secure the grid in place (Fig. 2F). At this point, the recording setup was complete and ready for signal acquisition (Fig. 2G). An overview of the teams' workflow process is shown in Supplementary Fig. A.

Electrophysiological Data Collection and Signal Processing

All microelectrode grids were placed after clinical passive HGM but before standard electrical stimulation mapping. Final grid placement was documented in 3D space by using a Stealth neuronavigation system and/or surgical microscope snapshots. Postuse channel yield and impedance data were collected in the OR after recordings were completed. Following use, microelectrode grids were resterilized and placed in storage.

Electrophysiological data were collected using an Intan 1024-channel recording system (Intan Technologies LLC) sampled at 20 or 30 kHz with a voltage scale of –5 mV to 5 mV at a time scale of 200 msec, or an ORH128 Intan recording system. The ORH128 Intan recording system data are acquired at 30 kHz and filtered by the default Intan setting, with cutoffs of 1 Hz to 7.5 kHz using the OpenEphys acquisition graphical user interface software (http://www.open-ephys.org/).[17] Electrode impedance testing during the experiments involved RHD2000 software from Intan Technologies. The Intan amplifier was set to

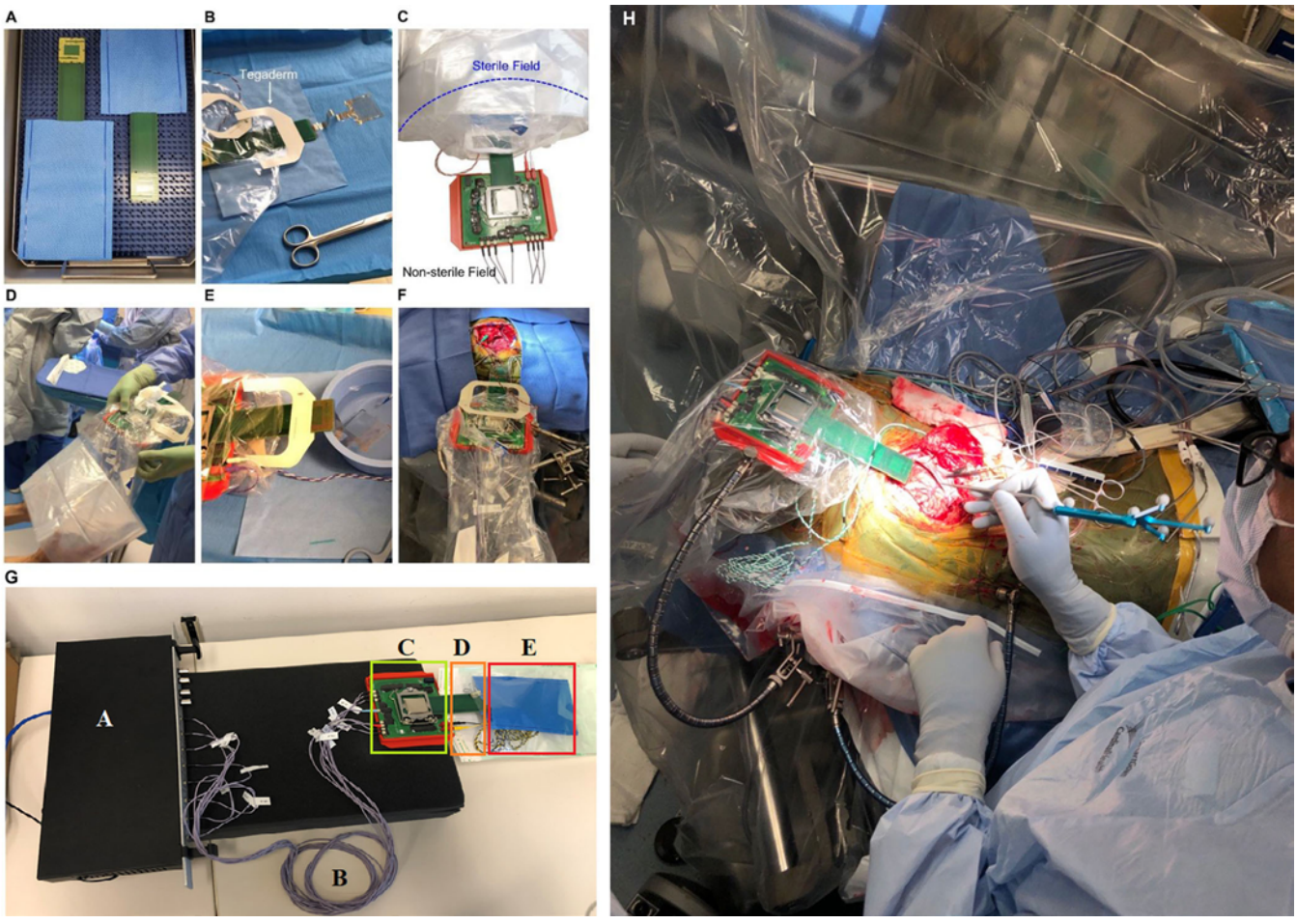

FIG. 2. A: Microelectrode grids in DuraHolder pouches placed in a sterilization tray. **B:** The extension board is passed through the Situate Sterile Drape and secured by Tegaderm to create a sterile barrier. **C and D:** The green extension board is then connected to an amplifier board (C) and the drape is then pulled from the inner, nonsterile surface by a team member such that it covers the amplifier board and associated outgoing cables (D). **E:** Impedance and channel yield testing is then performed with sterile saline. **F:** Once properly positioned, Greenberg or C clamps are used to secure the amplifier board in place. **G:** The recording setup. The Intan amplifier (*A*) is connected to the amplifier board via 8 serial peripheral interface cables (*B*). The amplifier board (*C*) is connected to the extension board and grid (*D* and *E*, respectively). **H:** Photograph showcasing the usage of microelectrode grids intraoperatively by the senior author. Panels A–F adapted from Tchoe Y, Bourhis AM, Cleary DR, et al. Human brain mapping with multithousand-channel PtNRGrids resolves spatiotemporal dynamics. *Sci Transl Med.* 2022, 14(628): eabj1441 (https://www.science.org/doi/10.1126/scitranslmed.abj1441). Reprinted with permission from AAAS. Figure is available in color online only.

a sampling rate of 20 kHz with a bandwidth of 7.6 kHz. Electrodes with more than 1000 channels were recorded with customized amplifier boards and Intan recording controllers were used to stream recorded data, which were spatially mapped with a recording laptop using in-house MATLAB scripts (MathWorks, Inc). Channels with impedance magnitudes higher than 100 kΩ in vivo at 1 kHz were excluded from analysis. Neighboring channels with diminished impedance magnitude were evaluated for potential short circuits. All recorded signals underwent removal of 60-Hz line noise and harmonics with digital notch filters. Offline analyses were conducted using custom, in-house scripts in MATLAB.

Statistical Analysis

Statistics were largely descriptive in nature and performed using GraphPad Prism version 9.0 software with a significance threshold of $\alpha = 0.05$. Categorical and dichotomous variables were reported as counts and percentages. Continuous variables were reported as the mean ± standard error or median (interquartile range), and were compared using nonparametric Mann-Whitney U-tests.

Results

Patient Demographics

Between January 1, 2019, and April 1, 2022, 89 patients had 94 grids placed during a craniotomy procedure for resection of pathological tissue. The mean patient age was 45.9 ± 1.7 years, with 63.0% and 24.7% undergoing operation at OHSU and MGH, respectively (Table 1). Resection of intracranial neoplasms was the most frequent indica-

TABLE 1. Demographic, clinical, operative, and intraoperative testing data in 89 patients who underwent craniotomy

Variable	Distribution & Frequency; n = 89 Pts*
Age in yrs	45.9 ± 1.7
Sex	
Male	47 (52.8)
Female	42 (47.2)
Institutional site	
OHSU	56 (63.0)
MGH	22 (24.7)
BWH	8 (9.0)
UCSD	3 (3.4)
Surgical indication	
Intracranial neoplasm	58 (65.2)
Intractable epilepsy	31 (34.8)
Preop deficits	
None	62 (69.7)
Motor	21 (23.6)
Visual field	7 (7.9)
Sensory	5 (5.6)
Language	4 (4.5)
Cognitive	3 (3.4)
Anesthesia	
Monitored anesthesia care	61 (68.5)
General anesthesia	28 (31.5)
Clinical mapping	
Phase reversal	45 (50.6)
Passive HGM	50 (56.2)
Electrical stimulation	52 (58.4)
Subcortical	11 (12.4)
Intracranial recording setting†	
Evoked response	11 (12.4)
Experimental task	52 (58.4)
Resting state	32 (36.0)
Functional domains tested	
Receptive language	32 (36.0)
Facial sensorimotor	5 (5.6)
Extremity sensorimotor	24 (27.0)
Visual	1 (1.1)
Not assessed	32 (36.0)
Research tasks	
Phonemic	30 (33.7)
Extremity motor/sensory	21 (23.6)
Facial motor/sensory	2 (2.2)
SSEP recording	17 (19.1)
Stimulation via electrode grid	8 (9.0)
Other/improvised	7 (7.9)
None	31 (34.8)

Pts = patients.
* Data are presented as the mean ± standard error or count (% of all patients) when applicable.
† Encompasses fence-post technique (n = 1) and subcortical stimulation (n = 1).

tion for surgery (65.2%). Most patients had no deficits preoperatively and underwent an awake craniotomy with monitored anesthesia care (68.5%) (Table 1).

Microelectrode Grids

Between January 1, 2019, and September 10, 2021, 36 PtNR grids were placed. Between January 1, 2019, and April 1, 2022, 58 PEDOT:PSS grids were placed. Overall, more 32 × 32–mm, 1024-channel grids (n = 48, 51.1%) were used, followed by 128-channel grids (n = 44, 46.8%). Two 2048-channel grids were used. Grid placement was informed by anatomical landmarks and hypothesis under evaluation, with temporal lobe regions being the most common (Table 2). There were 8 instances of PtNR grid failure across 7 patients, in whom either the cortical recordings obtained were unusable or cortical recording could not be performed altogether. Seven such instances were attributed to sterilization-related grid damage. One grid was damaged during sterile preparation in the OR after adhering to and ripping surgical gloves. Therefore, 86 of the 94 original grids were used to collect cortical recordings (Table 2).

Successful Cortical Data Collection and Experimental Testing

Cortical recordings were successfully obtained in 82 patients with 86 functioning grids. Four patients had cortical recordings performed with 2 grids. Grids were most frequently used for recording during experimental research tasks (58.4%) or with patients in a passive, resting state (Table 1). For those who did have functional testing, most underwent receptive language testing (36.0%) followed by extremity sensorimotor testing (27.0%). For patients who underwent research task paradigms, most participated in phonemic tasks (33.7%), followed by extremity motor and sensory tasks (23.6%) and passive SSEP recordings (19.1%) (Table 1).

V-PRO Sterilization Reduced Instances of PtNR Grid Dysfunction and Maximized Channel Yield

There were 8 instances of grid failure (Table 2). Seven instances involved 1024-channel PtNR grids and were attributed to grid damage during steam-based sterilization. For context, during the first few weeks, tap water steam–based autoclaving for PtNR grids was used. However, interinstitution differences (our personal observations, 2020) in channel yield and impedance were observed. These may be attributable to locale-specific variations in tap water mineral content. This prompted adoption of a V-PRO cycle involving aerosolization of hydrogen peroxide. Improvements in channel performance resulted and no further encounters or instances of intraoperative grid dysfunction were subsequently noted. Compared to steam-based sterilization, V-PRO conferred significantly superior channel yield (median 905 [IQR 650.8–935.5] vs 356 [IQR 18.0–597.8], p = 0.0031) for PtNR grids (Fig. 3).

PEDOT:PSS and PtNR Grids; Not Associated With Intraoperative or Postoperative Adverse Events

There were no instances of intraoperative adverse

TABLE 2. High-resolution microelectrode grid characteristics and use

Characteristic	Distribution & Frequency of Grid Use; n = 94 Grids*
Intraop grid use	
Success	86 (91.5)
Failure (PtNR grid)	8 (8.5)
Channel count & grid dimensions	
128 channels†	44 (46.8)
2 × 64–contact columns (50-μm pitch)	32
2 × 64–contact columns (800-μm pitch)	1
Circular, 4-mm diameter	11
1024 channels (32 × 32 mm)	48 (51.1)
2048 channels (48 × 48 mm)	2 (2.1)
Chemical composition	
PEDOT:PSS grid, n = 57 pts	58 (61.7)
PtNR grid, n = 25 pts	36 (38.3)
Grid placement‡	
Rolandic	10 (10.6)
Temporal lobe§	39 (41.5)
Posterior STG	12 (12.8)
Anterior STG	2 (2.1)
Temporoparietal	8 (8.5)
Extrarolandic parietal	4 (4.3)
Prefrontal lobe	10 (10.6)
Occipital	2 (2.1)
Overlying pathology	2 (2.1)
Multiple locations (relocated)	13 (13.8)
Placement strategy‡	
Anatomical landmarks	67 (71.3)
Passive HGM	18 (19.1)
Direct cortical stimulation	3 (3.2)
Recording duration (mins)	15.3 ± 1.15

* Frequencies are presented as mean ± standard error or count (% of all grids). Note that for categorical variables in which tallies for multiple categories can apply for a given patient, a percent is not given.
† Includes the 50-μm and 800-μm 2 × 64–contact column as well as the circular 128-channel grids.
‡ The 8 PtNR grid failures are not tallied and reported under these categories.
§ Includes posterior and anterior STG counts.

events or visible tissue damage related to PEDOT:PSS or PtNR grid use. Review of routine postoperative imaging revealed no focal abnormalities within or near the cortical regions overlaid by the grids, irrespective of grid material composition. Additionally, agnostic of grid material composition, there were no cases of postoperative cranial infections within 90 days after surgery.

Functional Mapping, Clinical Testing, and Intraoperative Neuromonitoring

In this patient cohort, in a patient undergoing awake tumor resection, a 1024-channel PtNR grid was placed over the central sulcus near where the hand region SSEPs were recorded (Fig. 4A). After stimulating peripheral nerves, waveforms with characteristic phase reversal reflective of the primary motor cortex–primary sensory cortex (M1-S1) functional boundary were captured using both 1024-channel PtNR grids and 2 × 8, 16-channel clinical ECoG grids. SSEPs captured on the PtNR grid had a maximum interpeak amplitude more than 20× greater than that of SSEPs captured on a clinical grid, and demonstrated a clear phase-reversal boundary. The PtNR grid allowed for visualization of the functional boundary between sensory and motor cortices relative to the canonical anatomical boundary (Fig. 4A). Both potential-based and correlation maps provided converging evidence of an offset curvilinear M1-S1 functional boundary indicative of pathological tissue–induced functional reorganization.

After phase-reversal mapping of the M1-S1 boundary, we attempted to map sensory and motor evoked cortical activity in the same patient. Using an experimental paradigm involving vibrotactile stimulation and a hand grasp task (Fig. 4B), the PtNR grid captured spatiotemporal dynamics of cortical motor and sensory activity with millimeter precision. Vibrotactile stimulation of fingertips elicited a focal increase in high gamma activity (HGA) in the S1. There were also spatially distinct patterns of HGA with stimulation of each of the individual fingertips, allowing us to discern neural correlates of motor activity through hand grasp trials (Fig. 4B). Cortical activity captured by the PtNR grid demonstrated that HGA began in the M1 before traveling to the M1-S1 functional boundary and ending in the S1, where it lingered after completion of the grasp motion (Fig. 4B).

In another patient with a temporal horn cavernoma undergoing a left temporal lobectomy for intractable epilepsy, the PtNR grid helped identify the seizure onset zone by capturing propagation patterns of seizure activity (Fig. 5A). Using vector fields and streamlines, we characterized the spatiotemporal dynamics of spontaneous and bipolar stimulation–induced seizure activity (Fig. 5B). We found that vector fields would gain coherence following both spontaneous and stimulation evoked ictal events. Epileptiform discharges would reliably propagate away from the site of stimulation origin following bipolar stimulation. Thus, for spontaneous seizure activity, the seizure onset zone could be inferred by tracing the propagated waveforms. For this patient, as indicated on the streamlines plot (Fig. 5B), spontaneous seizure activity originated from the right lower corner of the grid, closest to the cavernoma, implicating it as the source of ictal activity. These findings were congruent with the patient's prior stereoencephalography workup, and the epileptogenic tissue was resected as planned.

More recently, we used a 32 × 32–mm, 1-mm pitch PtNR grid and an auditory language testing paradigm to identify neural correlates of auditory language processing during an awake temporoparietal craniotomy for resection of a perirolandic neoplasm (Fig. 6A). A PtNR grid was placed over the patient's left inferior parietal lobe and superior temporal gyrus (STG) (Fig. 6B). Cortical activity captured by the PtNR grid during auditorily delivered English words was analyzed. We found a robust cortical

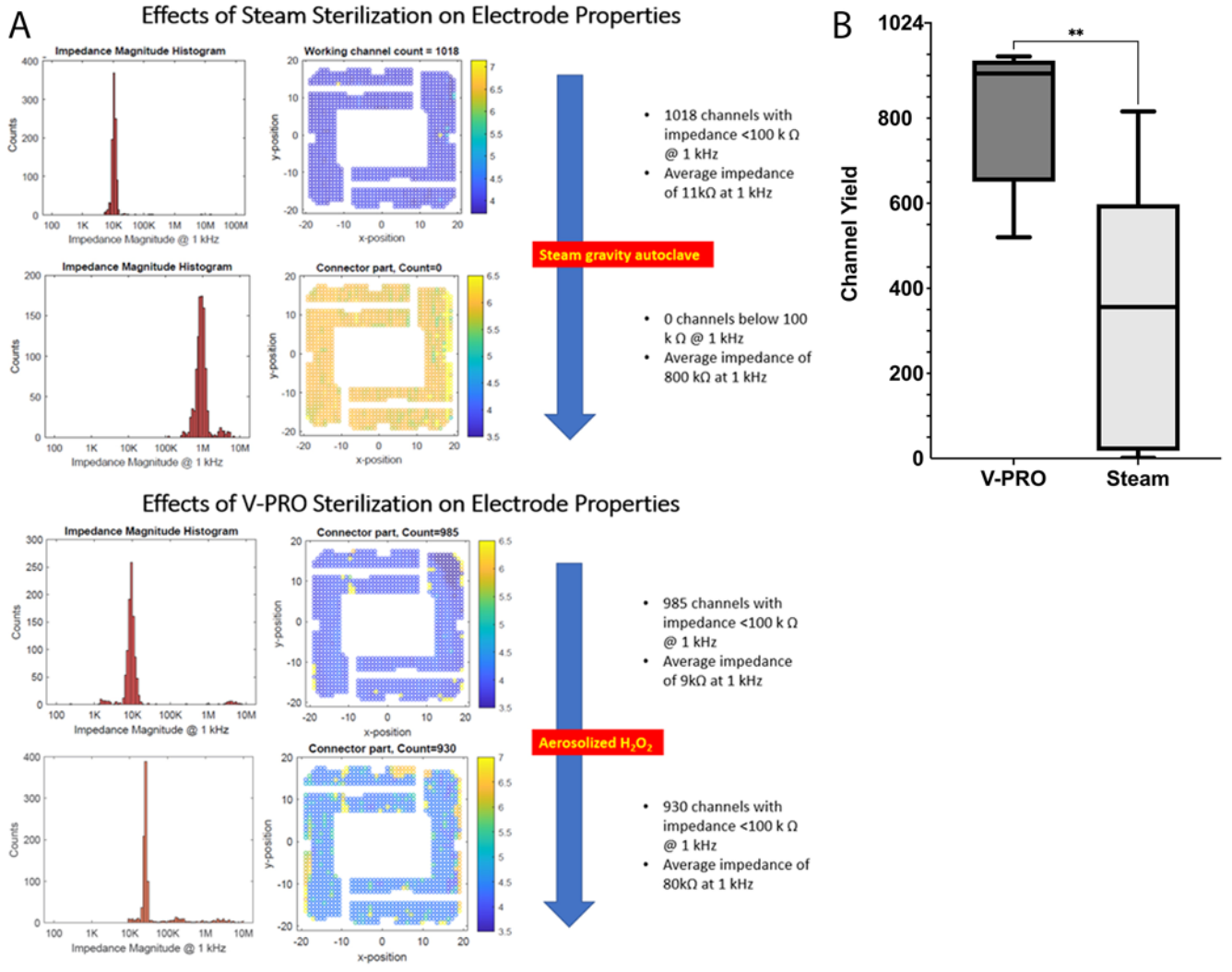

FIG. 3. Influence of sterilization modalities on PtNR grid impedance and channel yield. **A:** Exemplar outputs from an in-house MATLAB script used to conduct impedance and channel yield testing on PtNR grids. Note the greater median impedance magnitude increase (see impedance magnitude histograms) following steam autoclaving compared to V-PRO. **B:** Box plot showing the difference in usable channels following V-PRO and steam-based sterilization methods. Nonparametric Mann-Whitney U-test comparing channel yield of PtNR grids sterilized via steam (n = 7) versus V-PRO (n = 20) indicated that V-PRO preserved significantly more channels (median 905 [IQR 650.8–935.5] vs 356 [IQR 18.0–597.8], **p = 0.0031). Figure is available in color online only.

response to auditory word stimuli 500–600 msec after stimuli delivery. When the cortical response captured on the PtNR grid channels during word stimuli was averaged over this duration, a spatially distinct region of cortical activation could be discerned on the PtNR grid (Fig. 6C). Thus, using the PtNR grid, we were able to identify a region within the STG that demonstrated preferential engagement in response to auditory language stimuli.

Discussion

Increasing, improving, and refining ECoG grid resolution capabilities has broad clinical implications of interest to the neurosurgical and neuroscience community, and disease treatment implications for patients. The aim of this study was to demonstrate that the use of high-resolution electrode grids can be readily incorporated into a variety of standard of care practice and research settings if pertinent considerations are addressed.

Of the steps involved in the process of microelectrode grid use, we found that the most difficult was establishing a sterilization protocol for PEDOT:PSS grids versus PtNR grids. Uguz et al. and Tchoe et al. note that the optimal sterilization method seems to be dependent on the chemical composition of a given grid.[10,16] As such, we cannot overstate the importance of coordinating with hospital sterile materials processing staff to ensure that sterilization is conducted to optimize electrode performance. To date, no studies have compared the impact of different sterilization modalities on electrode grid parameters such as channel yield and impedance. However, for PtNR grids in particular, we strongly recommend V-PRO for steril-

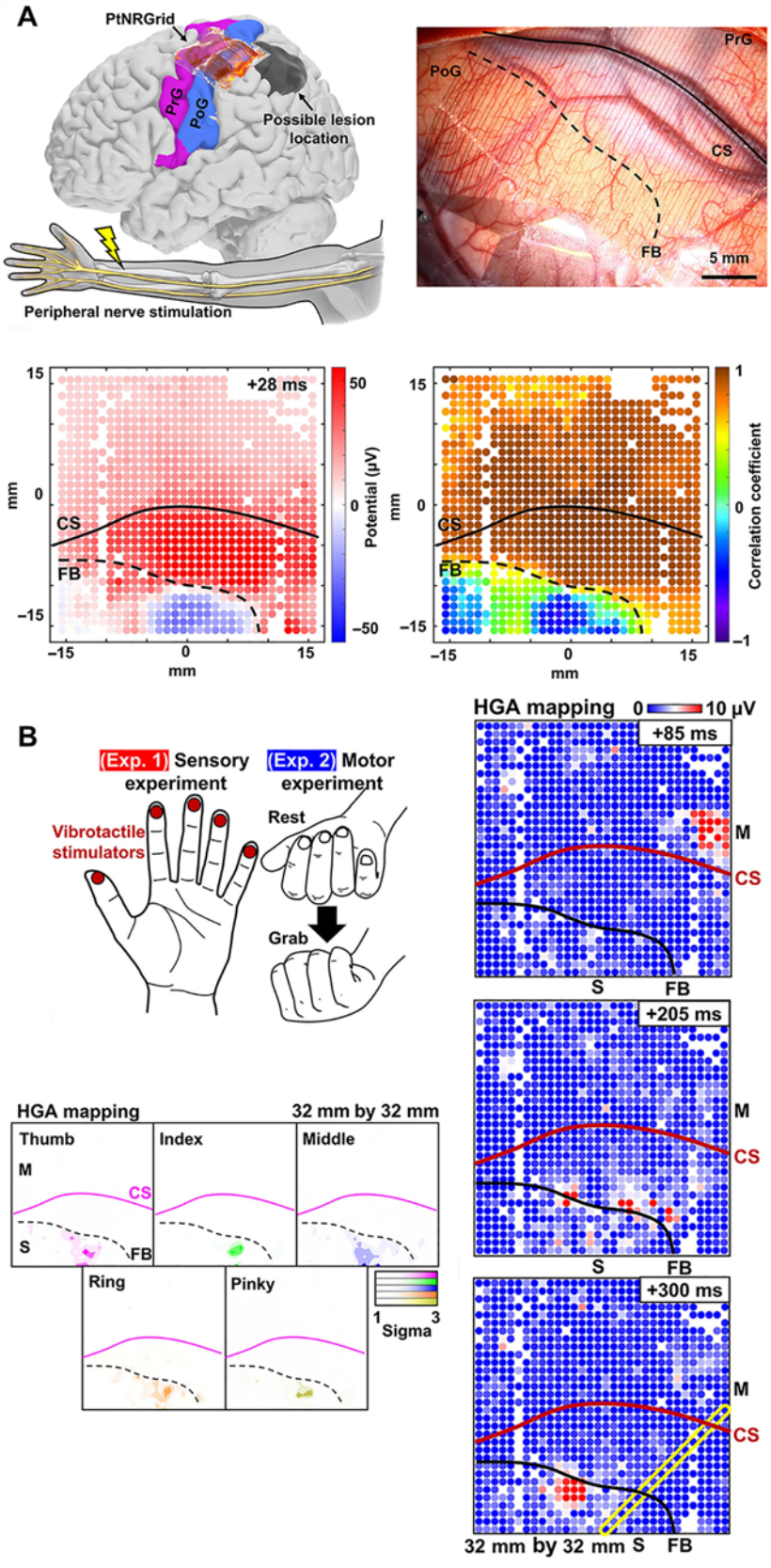

FIG. 4. A: PtNR microelectrode grid placement with the discrepancy in central sulcus versus phase reversal–identified M1-S1 functional boundary displayed. *Upper panels* show grid placement and the position of the identified functional boundary relative to the central sulcus, respectively. *Lower panels* show functional boundary versus central sulcus relationship identified through potential-based (*lower left*) and correlation coefficient (*lower right*) maps. **FIG. 4.** (*continued*)→

FIG. 4. B: Schematic of sensory and motor experimental paradigm with associated findings (*upper left*). A quintet of panels (*lower left*) shows the localization and intensity of HGA for each fingertip in response to vibrotactile stimulation. The 3 vertical panels (*right*) show the progression of HGA over the primary motor and sensory cortical regions at 85 msec, 205 msec, and 300 msec following hand grasp initiation. CS = central sulcus; FB = functional boundary; M = motor; PoG = postcentral gyrus; PrG = precentral gyrus; S = sensory. Adapted from Tchoe Y, Bourhis AM, Cleary DR, et al. Human brain mapping with multithousand-channel PtNRGrids resolves spatiotemporal dynamics. *Sci Transl Med.* 2022, 14(628): eabj1441 (https://www.science.org/doi/10.1126/scitranslmed.abj1441). Reprinted with permission from AAAS. Figure is available in color online only.

ization. Although there is nothing definitively erroneous per se about using other sterilization methods, V-PRO has performed the best for PtNR grids, in our experience, and is readily available at most institutions.

Importantly, throughout our experience, we encountered no instances of adverse events or intraoperative complications related to microelectrode grid use. This was not entirely unexpected given the diligent perioperative precautions and grid use that did not require the surgical team to make any substantial modifications, aside from added research time. Subjectively, patients better tolerated the microelectrode grids during passive cortical recording, because grids do not need to be pressed down to conform to cortical surface contours.

Notably, there were instances in which the PtNR grids did not function. These instances coincided with the time period immediately prior to implementation of V-PRO sterilization for PtNR grids, and could be attributed to electrode damage incurred during steam-based sterilization. Following the transition to V-PRO, there were no further instances of electrode failure prior to handling. This suggests that PtNR grids are reliable if sterilized appropriately before use.

The capacity to characterize cortical activity with millimeter precision could have significant implications for surgical management of neurological disorders. Higher-resolution ECoG setups may assist with improved demarcation of safe resection zones and mitigate the advent of functional deficits following surgeries that either involve or are near eloquent cortical regions.[5,6] This is especially valuable in the context of intracranial neoplastic processes as surgeons work to maximize resection extent to enhance survival without incurring functional deficits. Furthermore, intracranial neoplasms, particularly gliomas, are known to induce functional reorganization.[18–20] Tumor-induced reorganization may render conventional anatomical landmarks less reliable for functional localization, whereas contemporary mapping tools may have insufficient sensitivity.[21]

Recently, using PtNR grids Tchoe et al. better defined the M1-S1 cortical functional boundary, captured sensory and motor spatiotemporal dynamics, and recorded seizure onset and spread with millimeter precision.[10] Locating the functional boundary between motor and sensory cortices, which is commonly presumed to be central sulcus, is a critical surgical step, especially in the context of tumor resection.

M1-S1 functional boundary localization made possible by the microelectrode grids as described here demonstrates high-precision observation and measurements that would otherwise not have been accessible. In this particular example, shift of the functional boundary toward the postcentral sulcus indicated the presence of functional motor cortex tissue in the postcentral gyrus, which was critically important for the purpose of achieving safe resection. This shift in eloquent tissue was also confirmed with gold standard, direct electrical cortical stimulation of this area (data not presented). The postcentral gyrus is used as a surgical avenue for resection. If, in the cases we present, we had assumed location of eloquent tissues based on putative gross anatomical demarcations, postoperative functional deficits could have ensued. Although current neurosurgical microsurgery is not necessarily performed with millimeter precision, delineating boundaries of safe resection with millimeter resolution opens doors for new high-precision operative techniques in the future.

Obtaining cortical recordings at higher resolutions presents some technical challenges. Contemporary clinical grid systems rely primarily on clinical acumen and human interpretation of captured cortical spectral activity.[22] High-resolution grids necessitate use of an automated software-based analysis.[10] Given the high channel count of microelectrode grids, it would be impossible for humans to interpret captured electrophysiological activity. This represents a potential paradigm shift in real-time intraoperative mapping, with a gradual and increasing reliance on higher computational power, which parallels recent trends in biointerface technology advances.[23] This phenomenon of automated analysis of ECoG data is not entirely novel and is available commercially (CortiQ; g.tec)),[24] but at a more modest resolution, and requires clinical contextualization. Should high-channel-count micro-ECoG be used ultimately for intraoperative functional cortical localization, processing the vast amounts of cortical recording data in near real time would likely be possible only through advancement in computing capability.[23]

Brain–computer interface (BCI) represents another intriguing window of opportunity for microelectrode grid use. BCI configurations that use current clinical ECoG grids are limited by modest spatial resolution.[25] However, the microelectrodes described here are capable of capturing brain activity with robust spatial resolution over a physiologically relevant area of the cortex,[10] representing a dramatic improvement from recordings obtained in previous micro- and macro-ECoG configurations.[26,27] This allows for better characterization of the spatiotemporal dynamics unique to individual patients and should enhance BCI operations. Importantly, whether the PtNR grids described here are safe for the long-term implantation required of a BCI has yet to be investigated. Further investigation is needed to evaluate the safety profile of microelectrode grids to assess their suitability as potential neuroprostheses.

In our experience, we were able to integrate microelectrode grids seamlessly into surgical workflow. However, we stress and emphasize that successful incorporation of microelectrode grids into care is contingent on strong multidisciplinary collaboration between research, clinical, and

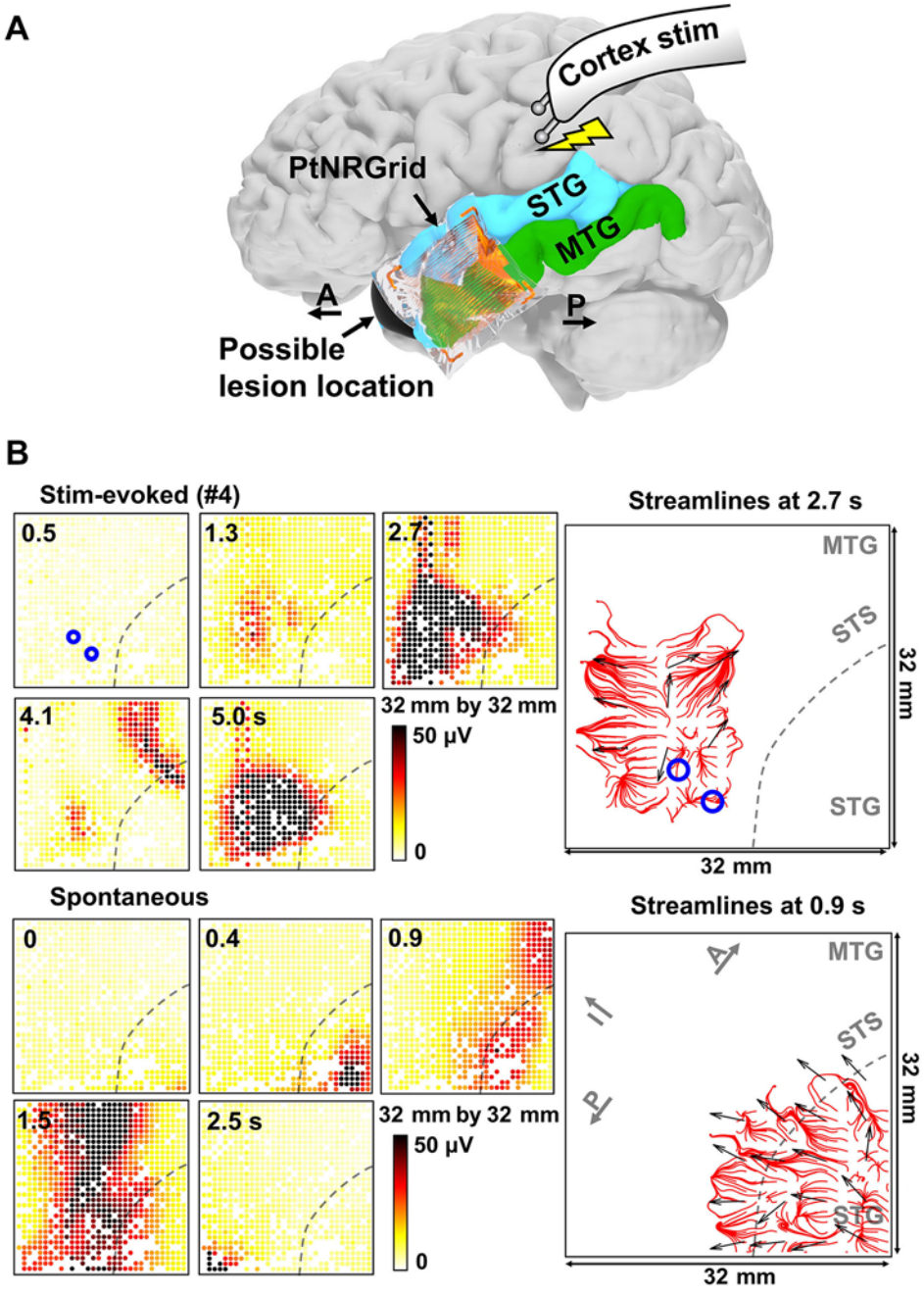

FIG. 5. A: PtNR microelectrode grid placement relative to the potential seizure focus, STG and middle temporal gyrus (MTG). **B:** Stimulation-induced and spontaneous ictal cortical discharges captured on the PtNR grid. *Left-hand panels* show temporal changes in stimulation and spontaneous evoked brain wave amplitudes, whereas *right-hand panels* feature streamlines plots, with *arrows* indicating the direction of brain wave spread. *Blue circles* designate bipolar stimulator contact points on the cortex. A = anterior; P = posterior; STS = superior temporal sulcus. Adapted from Tchoe Y, Bourhis AM, Cleary DR, et al. Human brain mapping with multithousand-channel PtNRGrids resolves spatiotemporal dynamics. *Sci Transl Med.* 2022, 14(628): eabj1441 (https://www.science.org/doi/10.1126/scitranslmed.abj1441). Reprinted with permission from AAAS. Figure is available in color online only.

ancillary staff. Additionally, development of a consistent workflow from order placement to postoperative recovery is imperative.

Study Limitations

We present data obtained in the first series of patients, to our knowledge, to undergo intraoperative cortical recording with high-resolution microelectrode grids during a craniotomy for pathological tissue resection. The study is limited by the inherent bias of a retrospective design. Although this was a multiinstitution study, some biases may have affected the results because of patient volume at

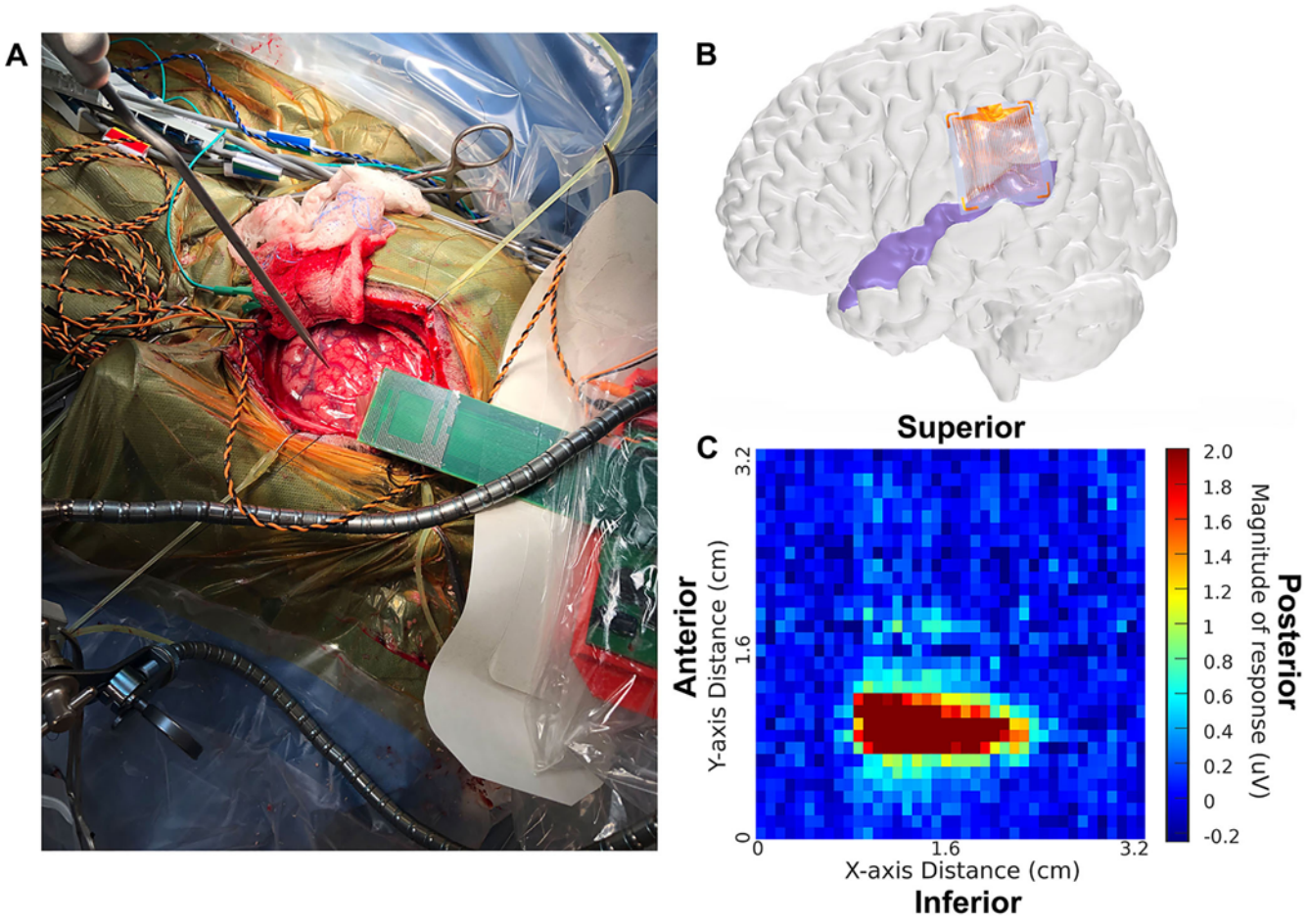

FIG. 6. A: Intraoperative photograph showing the placement of the PtNR microelectrode grid in relation to the temporoparietal craniotomy. **B:** Illustration depicting the placement of the PtNR grid in relation to the STG, which is colored *light purple*. **C:** Heat map showing the degree of mean cortical response 500–600 msec after auditory language stimuli delivery across PtNR grid channels. Note the horizontal oblong region of particularly strong response shown in *dark red*. Figure is available in color online only.

individual institutions. Although our interpretation of the results is that high-spatial-resolution grids will outperform standard clinical grids with regard to spatial resolution, there were no experimental design comparisons, nor were clinical decisions made based on microelectrode findings. All analyses were post hoc. A guide for grid use is provided; however, we do not provide an overview of how to analyze recorded neurophysiological data. An overview of spectral analysis techniques is beyond the scope of this article. We refer readers to other comprehensive publications related to this subject.[28] Future investigations will assist with further clarification regarding the clinical utility of microelectrode grids and better characterize the diagnostic value of high-resolution grids compared to current clinical grids.

Conclusions

High-spatial-resolution microelectrode grids for cortical mapping can be readily incorporated into neurosurgical craniotomy procedures. Microelectrode grids can potentially provide clinically relevant information about patients and better inform surgical planning. Nonetheless, analyses of postsurgical outcomes following the intraoperative use of these grids will better characterize their clinical value. Special attention to preoperative handling and sterilization processes helps preserve the number of usable channels and optimizes recording resolution. Further investigations are needed to compare the diagnostic value of these grids to that of clinical grids and to extrapolate whether potential diagnostic differences relate to clinical outcomes.

Acknowledgments

We received funding from DHHS NIH National Institute of Neurological Disorders and Stroke (NINDS; grant no. 1UG3NS123723-01); see https://reporter.nih.gov/search/ssKtOcBsUEqLymCbavnJLA/project-details/10294893?. We also thank Shirley McCartney, PhD, for editorial assistance.

References

1. Morshed RA, Young JS, Lee AT, Hervey-Jumper SL. Functional mapping for glioma surgery, part 2: intraoperative mapping tools. *Neurosurg Clin N Am*. 2021;32(1):75-81.
2. Ille S, Krieg SM. Functional mapping for glioma surgery,

part 1: Preoperative mapping tools. *Neurosurg Clin N Am*. 2021;32(1):65-74.
3. Crone NE, Sinai A, Korzeniewska A. High-frequency gamma oscillations and human brain mapping with electrocorticography. *Prog Brain Res*. 2006;159:275-295.
4. Roland JL, Hacker CD, Leuthardt EC. A review of passive brain mapping techniques in neurological surgery. *Neurosurgery*. 2020;88(1):15-24.
5. Sinai A, Bowers CW, Crainiceanu CM, et al. Electrocorticographic high gamma activity versus electrical cortical stimulation mapping of naming. *Brain*. 2005;128(Pt 7):1556-1570.
6. Kojima K, Brown EC, Rothermel R, et al. Clinical significance and developmental changes of auditory-language-related gamma activity. *Clin Neurophysiol*. 2013;124(5):857-869.
7. Maynard EM, Nordhausen CT, Normann RA. The Utah Intracortical Electrode Array: a recording structure for potential brain-computer interfaces. *Electroencephalogr Clin Neurophysiol*. 1997;102(3):228-239.
8. Ganji M, Elthakeb AT, Tanaka A, Gilja V, Halgren E, Dayeh SA. Scaling effects on the electrochemical performance of poly (3, 4-ethylenedioxythiophene (PEDOT), Au, and Pt for electrocorticography recording. *Adv Funct Mater*. 2017; 27(42):1703018.
9. Ganji M, Paulk AC, Yang JC, et al. Selective formation of porous Pt nanorods for highly electrochemically efficient neural electrode interfaces. *Nano Lett*. 2019;19(9):6244-6254.
10. Tchoe Y, Bourhis AM, Cleary DR, et al. Human brain mapping with multithousand-channel PtNRGrids resolves spatiotemporal dynamics. *Sci Transl Med*. 2022;14(628):eabj1441.
11. Yang JC, Paulk AC, Salami P, et al. Microscale dynamics of electrophysiological markers of epilepsy. *Clin Neurophysiol*. 2021;132(11):2916-2931.
12. Paulk AC, Yang JC, Cleary DR, et al. Microscale physiological events on the human cortical surface. *Cereb Cortex*. 2021; 31(8):3678-3700.
13. von Elm E, Altman DG, Egger M, Pocock SJ, Gøtzsche PC, Vandenbroucke JP. The Strengthening the Reporting of Observational Studies in Epidemiology (STROBE) statement: guidelines for reporting observational studies. *Ann Intern Med*. 2007;147(8):573-577.
14. Hermiz J, Rogers N, Kaestner E, et al. Sub-millimeter ECoG pitch in human enables higher fidelity cognitive neural state estimation. *Neuroimage*. 2018;176:454-464.
15. Ganji M, Hossain L, Tanaka A, et al. Monolithic and scalable Au nanorod substrates improve PEDOT–metal adhesion and stability in neural electrodes. *Adv Healthc Mater*. 2018;7(22): e1800923.
16. Uguz I, Ganji M, Hama A, et al. Autoclave sterilization of PEDOT:PSS electrophysiology devices. *Adv Healthc Mater*. 2016;5(24):3094-3098.
17. Siegle JH, López AC, Patel YA, Abramov K, Ohayon S, Voigts J. Open Ephys: an open-source, plugin-based platform for multichannel electrophysiology. *J Neural Eng*. 2017;14(4): 045003.
18. Kristo G, Raemaekers M, Rutten GJ, de Gelder B, Ramsey NF. Inter-hemispheric language functional reorganization in low-grade glioma patients after tumour surgery. *Cortex*. 2015;64:235-248.
19. Charras P, Herbet G, Deverdun J, et al. Functional reorganization of the attentional networks in low-grade glioma patients: a longitudinal study. *Cortex*. 2015;63:27-41.
20. Yang J, Kudulaiti N, Chen Z, et al. Within and beyond the visual cortex: brain tumors induce highly sensitive plasticity of visual processing in whole-brain neural functional networks. *Cereb Cortex*. 2022;32(20):4422-4435.
21. Hong G, Lieber CM. Novel electrode technologies for neural recordings. *Nat Rev Neurosci*. 2019;20(6):330-345.
22. Korostenskaja M, Kamada K, Guger C, et al. Electrocorticography-based real-time functional mapping for pediatric epilepsy surgery. *J Pediatr Epilepsy*. 2015;4(4):184-206.
23. Lebedev MA, Nicolelis MA. Brain-machine interfaces: past, present and future. *Trends Neurosci*. 2006;29(9):536-546.
24. Prueckl R, Kapeller C, Potes C, et al. cortiQ—Clinical software for electrocorticographic real-time functional mapping of the eloquent cortex. *Annu Int Conf IEEE Eng Med Biol Soc*. 2013;2013:6365-6368.
25. Schalk G, Leuthardt EC. Brain-computer interfaces using electrocorticographic signals. *IEEE Rev Biomed Eng*. 2011;4: 140-154.
26. Rubino D, Robbins KA, Hatsopoulos NG. Propagating waves mediate information transfer in the motor cortex. *Nat Neurosci*. 2006;9(12):1549-1557.
27. Muller L, Piantoni G, Koller D, Cash SS, Halgren E, Sejnowski TJ. Rotating waves during human sleep spindles organize global patterns of activity that repeat precisely through the night. *eLife*. 2016;5:e17267.
28. Mercier MR, Dubarry AS, Tadel F, et al. Advances in human intracranial electroencephalography research, guidelines and good practices. *Neuroimage*. 2022;260:119438.

Disclosures

Dr. Tchoe reported equity in Precision Neurotek Inc. outside the submitted work. Mr. Bourhis reports a patent pending for "Multi-Thousand Channel Electrode Electrophysiological Array and Fabrication Method." Dr. Halgren reported membership on the scientific advisory board of Cortechs.ai outside the submitted work. Dr. Dayeh reported a patent (WO2020097305A1) pending; and that he cofounded Precision Neurotek to commercialize the PtNR grid.

Author Contributions

Conception and design: Raslan, Stedelin, Cleary, Nerison, Tchoe, Ro, Ganji, Siler, Han, Ben-Haim, Halgren, Cash, Dayeh. Acquisition of data: Raslan, Tan, Paulk, Stedelin, Cleary, Nerison, Tchoe, Brown, Bourhis, Russman, J Lee, Tonsfeldt, Yang, Oh, Siler, Collins, Halgren, Cash, Dayeh. Analysis and interpretation of data: Raslan, Tan, Tchoe, Brown, Bourhis, Tonsfeldt, Han, Halgren, Dayeh. Drafting the article: Raslan, Tan, Stedelin, Cleary, J Lee, Dayeh. Critically revising the article: Raslan, Tan, Paulk, Brown, Yang, Han, Collins, Ben-Haim, Cash, Dayeh. Reviewed submitted version of manuscript: Raslan, Tan, Nerison, Brown, Bourhis, Russman, J Lee, Yang, Han, Collins, Ben-Haim, Halgren, Cash, Dayeh. Approved the final version of the manuscript on behalf of all authors: Raslan. Statistical analysis: Raslan, Tan. Administrative/technical/material support: Raslan, Paulk, Stedelin, Cleary, Nerison, J Lee, K Lee, Galton, Collins, Halgren, Dayeh. Study supervision: Raslan, Han, Dayeh.

Supplemental Information

Online-Only Content

Supplemental material is available with the online version of the article.

Supplementary Fig. A. https://thejns.org/doi/suppl/10.3171/2023.7.JNS23885.

Correspondence

Ahmed M. Raslan: Oregon Health & Science University, Portland, OR. raslana@ohsu.edu.